

NUMERICAL SIMULATION OF A RADIAL DIFFUSOR AIRFLOW CONSIDERING DIFFERENT TURBULENCE MODELS AND COMPUTATIONAL PARAMETERS

Alysson Kennerly Colaciti

Tecumseh do Brasil LTDA, Product Research & Development. Rua Cel. J.A. de Oliveira Salles, 478, Caixa Postal 54 – CEP 13560-971, São Carlos – SP - Brasil
Alyssonkennerly@gmail.com

Luis Miguel Valdés López

Tecumseh do Brasil LTDA, Product Research & Development. Rua Cel. J.A. de Oliveira Salles, 478, Caixa Postal 54 – CEP 13560-971, São Carlos – SP - Brasil
llopez@tecumseh.com.br

Luben Cabezas Gómez

Tecumseh do Brasil LTDA, Product Research & Development. Rua Cel. J.A. de Oliveira Salles, 478, Caixa Postal 54 – CEP 13560-971, São Carlos – SP - Brasil
lcabezas@tecumseh.com.br

Abstract. In the present work are presented results from numerical simulations performed with the ANSYS-CFX[®] code. It is studied a radial diffuser flow case, which is the main academic problem used to study the flow behavior on flat plate valves. The radial flow inside the diffuser has important behaviors such as the turbulence decay downstream and recirculation regions inside the valve flow channel due to boundary layer detachment. These flow structures are present in compressor reed valves configurations, influencing in a greater extent the compressor efficiency. The main target of the present paper was finding the simulation set-up (computational domain, boundary conditions and turbulence model) that better fits with experimental data published by Tabatabai and Pollard (1987). The local flow turbulence and velocity profiles were investigated using four different turbulence models, two different boundary conditions set-up, two different computational domains and three different flow conditions (Re_{in} – Reynolds number at the diffuser inlet). Where used the Baseline (BSL) $k-\omega$; the $k-\epsilon$; the RNG $k-\epsilon$; and the Shear Stress Transport (SST) $k-\omega$ turbulence models. The performed computational results analysis and comparison with experimental data show that the choice of the turbulence model, as well as, the choice of the other computational conditions, play an important role on results physical quality and accuracy.

Keywords. Radial diffuser flow, turbulence models, numerical simulation, ANSYS-CFX[®] code

1. Introduction

Radial outward flow between stationary disks has industrial and scientific applications such as in radial diffusers (present in hermetic compressor reed valves), non-rotating air bearings and disk-type heat exchangers. Such flows are rather complex, having a pressure gradient either positive or negative depending on the radial location and radius values. A positive pressure gradient, resulting from a decrease in the velocity with increasing radius, may lead to separation and secondary flows. In some cases, a flow that starts as turbulent flow may revert to laminar flow at some distance downstream (Tabatabai and Pollard, 1987; Ervin *et al.*, 1989).

Many investigations have been performed to study the laminar radial flow between parallel disks. For example, Livesey (1960), Moller (1963), Savage (1964), Jackson and Symmons (1965), among others, developed analytical and experimental studies, while Hayashi *et al.* (1975), Raal (1978), and Piechna and Meier (1986) among others, developed numerical studies with the same aim. After that, other investigations were performed to study how behaves a turbulent radial flow between parallel disks. Two important experimental works concerning this kind of study are those developed by Tabatabai and Pollard (1987) and Ervin *et al.* (1989).

Recently, many other works has been developed to study more deeply the flow inside radial diffusers taking advantage of the flow details that Computational Fluid Dynamics (CFD) techniques allows to obtain. Cyklis (1994) investigate the suitability of CFD techniques for analysis of compressor valves. Using a simplified geometry of compressor valve consisting of a radial diffuser with axial feeding was computed the steady planar mass-flow rate as a function of pressure difference, being the results slightly lower than measured data. Deschamps *et al.* (1996) considered a turbulent flow using the Renormalization Group $k-\epsilon$ model and fixed walls. The pressure distribution along the frontal disc showed good agreement with experimental data, for different valve openings and Reynolds numbers. With this work the authors obtained some flow details that were not possible to obtain with the previous models used in Deschamps *et al.* (1988 and 1989), where they used the $k-\epsilon$ model for high Reynolds numbers and two versions of the $k-\epsilon$ models for low Reynolds numbers.

In 1999, Perez-Segarra *et al.* (1999) considering three different versions of the $k-\varepsilon$ model showed significant differences in computed flow force and effective flow area. This agrees with the comparison of Ottitsch and Scarpinato (2000) developed for different types of valves. In a next step in using CFD techniques for compressor valves Matos *et al.* (1999) simulated the fluid-structure interaction. The authors considered an axis-symmetric laminar flow around a circular plate with prescribed pressure difference. The structure was modeled as a mass-spring system with a single degree of freedom. The gas force was found to be in phase with the harmonically varying pressure difference, except near valve closure when this force experiences a temporary drop. When both pressure difference and flow force become negative, the mass-flow rate at the exit becomes negative too.

Possamai *et al.* (2001) computed laminar flow between concentric inclined disks and conclude that this flow is significantly affected by the inclination for inclinations as small as 0.1° . For some combinations of Reynolds number, valve opening and inclination, the pressure distribution showed regions of negative pressure difference, which produce a restoring moment tending to force the disks to become parallel. In the work of Matos *et al.* (2002) was computed an axi-symmetric turbulent flow around a circular plate, which was modeled as a mass-spring system. CFD techniques, along with other techniques, also were applied by Having (2005), which presents a very detailed study about the flow through compressor valves.

In the present paper four turbulence models are tested, comparing the obtained simulation results for a radial air diffuser flow with the experimental data of Tabatabai and Pollard (1987). The influence of three computational parameters over the simulation results also is addressed in the present paper. These parameters include, the type of boundary condition at the lateral walls of the computational domain, the type of the employed computational geometry, and the inlet flow conditions through the inlet Reynolds number. Among the tested models the shear stress transport (SST) model proposed by Menter (1994) and implemented into the ANSYS-CFX[®] code, seems to be the best compromise for obtaining a good quality results with a reasonable computational cost. In the next section are presented the balance equations of each turbulence model.

2. Mathematical model

In the present paper are used four different turbulence models. Three of them are a two-equations turbulence models, namely the traditional $k-\varepsilon$ model, the *RNG* $k-\varepsilon$ model and the *SST* model, obtained by Menter (1994) from the $k-\omega$ turbulence model, initially formulated by Wilcox (1993). The other turbulence model is a version of the Reynolds Stress Turbulence kind of model, using a differential equation to compute the Reynolds stresses. The models are presented in the above-mentioned order, considering only the main equations used in the numerical simulations. Models constants are also introduced. It is important to note that are presented the model definitions and formulation used in the ANSYS-CFX[®] manual (2006), because the numerical simulations were performed with this commercial code. The main interest is to study how different models can lead to very different computational results only considering the defaults definition of each model, including the default boundary conditions.

2.1 $k-\varepsilon$ model

The standard $k-\varepsilon$ model (see Launder and Spalding, 1974) introduces two new variables into the equation system. One is for the computation of the turbulent kinetic energy, k , m^2/s^2 ; and the other is for the calculation of the turbulence eddy dissipation, ε , m^2/s^3 . The following equations are then obtained:

Continuity equation:

$$\frac{\partial \rho}{\partial t} + \nabla \cdot (\rho U) = 0 \quad (1)$$

Momentum equation:

$$\frac{\partial(\rho U)}{\partial t} + \nabla \cdot (\rho U \otimes U) = -\nabla p' + \nabla \cdot (\mu_{eff} (\nabla U + (\nabla U)^T)) + B \quad (2)$$

where B is the sum of body forces, μ_{eff} is the effective viscosity accounting for turbulence, and p' is the modified pressure. μ_{eff} and p' are given respectively by:

$$\mu_{eff} = \mu + \mu_t \quad (3)$$

$$p' = p + \frac{2}{3} \rho k \quad (4)$$

The k - ε model uses the eddy viscosity concept, assuming that the turbulence viscosity is computed by:

$$\mu_t = C_\mu \rho \frac{k^2}{\varepsilon} \quad (5)$$

where C_μ is a model constant.

The quantities k and ε are computed directly from the resolution of the following differential transport equations:

$$\frac{\partial(\rho k)}{\partial t} + \nabla \cdot (\rho U k) = \nabla \cdot \left[\left(\mu + \frac{\mu_t}{\sigma_k} \right) \nabla k \right] + P_k - \rho \varepsilon \quad (6)$$

$$\frac{\partial(\rho \varepsilon)}{\partial t} + \nabla \cdot (\rho U \varepsilon) = \nabla \cdot \left[\left(\mu + \frac{\mu_t}{\sigma_\varepsilon} \right) \nabla \varepsilon \right] + \frac{\varepsilon}{k} (C_{\varepsilon 1} P_k - C_{\varepsilon 2} \rho \varepsilon) \quad (7)$$

being $C_{\varepsilon 1}$, $C_{\varepsilon 2}$, σ_k and σ_ε model constants and P_k is the turbulence production due to viscous forces. The buoyancy forces are not considered in the present work. This last term is modeled as:

$$P_k = \mu_t \nabla U \cdot (\nabla U + \nabla U^T) - \frac{2}{3} \nabla \cdot U (3\mu_t \nabla \cdot U + \rho k) \quad (8)$$

If the flow is incompressible, $\nabla \cdot U$ is very small. In this case the second term of the Eq. (8) does not contribute to the turbulence production. In the present simulations the flow is considered compressible and all these terms are taken into account. The standard k - ε model employs values for the constants that were found by a comprehensive data fitting for a wide range of turbulent flows. The values of these constants are:

$$C_\mu = 0.09; C_{\varepsilon 1} = 1.44; C_{\varepsilon 2} = 1.92; \sigma_k = 1.00; \text{ and } \sigma_\varepsilon = 1.30 \quad (9)$$

2.2 RNG k - ε model

The *RNG* k - ε model is based on renormalization group analysis of the Navier-Stokes equations (Yakhot et al., 1992). The transport equations for turbulence generation and dissipation are the same as those for the standard k - ε model, but the model constants differ. The equations for the momentum and continuity are also the same.

For the *RNG* k - ε model the transport equation for turbulence dissipation becomes:

$$\frac{\partial(\rho \varepsilon)}{\partial t} + \nabla \cdot (\rho U \varepsilon) = \nabla \cdot \left[\left(\mu + \frac{\mu_t}{\sigma_{\varepsilon RNG}} \right) \nabla \varepsilon \right] + \frac{\varepsilon}{k} (C_{\varepsilon 1 RNG} P_k - C_{\varepsilon 2 RNG} \rho \varepsilon) \quad (10)$$

where

$$C_{\varepsilon 1 RNG} = 1.42 - f_\eta \quad (11)$$

and

$$f_\eta = \frac{\eta \left(1 - \frac{\eta}{4.38} \right)}{\left(1 + \beta_{RNG} \eta^3 \right)}; \eta = \sqrt{\frac{P_k}{\rho C_{\mu RNG} \varepsilon}} \quad (12a,b)$$

The values of the constants are:

$$C_{\mu RNG} = 0.085; C_{\varepsilon 2 RNG} = 1.68; \sigma_{k RNG} = 0.7179; \text{ and } \sigma_{\varepsilon RNG} = 0.7179 \quad (13)$$

2.3 SST model

The other two-equations turbulence model refers to the Shear Stress Transport (SST) model of the ANSYS-CFX[®] manual (2006). This model was proposed by Menter (1994), and grew from the denominated Baseline $k-\omega$ model (see the ANSYS-CFX[®] manual, 2006). The Baseline $k-\omega$ model makes use of the $k-\varepsilon$ model in regions far away from the walls and the $k-\omega$ Wilcox model near the surface (Wilcox, 1993). The SST model is an improvement of the Baseline $k-\omega$ model, taking into account the transport of the turbulent shear stress by a limitation of the eddy viscosity ν_t by the following equation:

$$\nu_t = \frac{a_1 k}{\max(a_1 w, SF_2)} \quad (14)$$

where: $\nu_t = \mu_t / \rho$ and S represents an invariant measure of the strain rate. F_2 is a blending function, which restricts the limiter to the wall layer computed by:

$$F_2 = \tanh(\arg_2^2) \quad (15)$$

with:

$$\arg_2 = \max\left(\frac{2\sqrt{k}}{\beta' w y}, \frac{500\nu}{y^2 w}\right) \quad (16)$$

The turbulent kinetic energy, k and turbulent frequency, ω are computed by the following relations:

$$\frac{\partial(\rho k)}{\partial t} + \nabla \cdot (\rho U k) = \nabla \cdot \left[\left(\mu + \frac{\mu_t}{\sigma_{k3}} \right) \nabla k \right] + P_k - \beta' \rho k \omega \quad (17)$$

$$\frac{\partial(\rho \omega)}{\partial t} + \nabla \cdot (\rho U \omega) = \nabla \cdot \left[\left(\mu + \frac{\mu_t}{\sigma_{\omega 3}} \right) \nabla \omega \right] + (1 - F_2) 2\rho \frac{1}{\sigma_{\omega 2} \omega} \nabla k \nabla \omega + \alpha_3 \frac{\omega}{k} P_k - \beta_3 \rho \omega^2 \quad (18)$$

The constants used in the SST model equations are:

$$\begin{aligned} \beta' &= 0.09; \alpha_1 = 5/9; \beta_1 = 0.075; \sigma_{k1} = 2; \sigma_{\omega 1} = 2; \\ \alpha_2 &= 0.44; \beta_2 = 0.0828; \sigma_{k2} = 1; \text{ and } \sigma_{\omega 2} = 1/0.856 \end{aligned} \quad (19)$$

The coefficients of the SST model are a linear combination of the corresponding coefficients of the underlying models:

$$\Phi_3 = F_2 \Phi_1 + (1 - F_2) \Phi_2 \quad (20)$$

It should be noted that the stress tensor is computed from the eddy-viscosity concept. Is used the Eq. (1) for the conservation of mass.

2.4 Reynolds Stress Turbulence (BSL) model

The last model considered in this paper is the Reynolds Stress Turbulence model. This kind of model is based on transport equations for all components of the Reynolds stress tensor and dissipation rate. The eddy viscosity concept is not used, and is solved an equation for the transport of Reynolds stresses in fluid. The transport equations are solved for the individual stress components. In the present model is used a differential equation for the Reynolds stress transport computation, based on the turbulence frequency ω . As the turbulence frequency ω is computed using the Baseline $k-\omega$ model, the present Reynolds Stress model is denominated as the BSL Reynolds Stress model following the ANSYS-

CFX[®] manual denomination. There are various Reynolds stress turbulence models as those published by Launder *et al.* (1975) and Speziale *et al.* (1991). The present *BSL* model has some differences in relations to these models. In this case the modeled equation for the Reynolds stresses are written as:

$$\frac{\partial(\rho\tau_{ij})}{\partial t} + \frac{\partial(U_k \rho\tau_{ij})}{\partial x_k} = -\rho P_{ij} + \frac{2}{3}\beta' \rho \omega k \delta_{ij} - \rho \Pi_{ij} + \frac{\partial}{\partial x_k} \left(\left(\mu + \frac{\mu_t}{\sigma^*} \right) \frac{\partial \tau_{ij}}{\partial x_k} \right) \quad (21)$$

where the constitutive relation for the pressure-strain correlation is given by:

$$\Pi_{ij} = \beta' C_1 \omega \left(\tau_{ij} + \frac{2}{3} k \delta_{ij} \right) - \hat{\alpha} \left(P_{ij} - \frac{2}{3} P \delta_{ij} \right) - \hat{\beta} \left(D_{ij} - \frac{2}{3} P \delta_{ij} \right) - \hat{\gamma} k \left(S_{ij} - \frac{1}{3} S_{kk} \delta_{ij} \right) \quad (22)$$

The production tensor of Reynolds stresses is given by:

$$P_{ij} = \tau_{ik} \frac{\partial U_j}{\partial x_k} + \tau_{jk} \frac{\partial U_i}{\partial x_k}; \text{ and } P = \frac{1}{2} P_{kk} \quad (23a,b)$$

The tensor D term only differs from the above equation in the dot-product indices:

$$D_{ij} = \tau_{ik} \frac{\partial U_k}{\partial x_j} + \tau_{jk} \frac{\partial U_k}{\partial x_i} \quad (24)$$

The turbulent viscosity in the diffusion terms of the balance equations of the Reynolds stresses equation is computed as in the Wilcox (1993) *k- ω* model:

$$\mu_t = \rho \frac{k}{\omega} \quad (25)$$

In the above equations the constant coefficients are equal to:

$$\beta' = 0.09; \hat{\alpha} = (8 + C_2)/11; \hat{\beta} = (8C_2 - 2)/11; \hat{\gamma} = (60C_2 - 4)/55; C_1 = 1.8; C_2 = 0.52 \quad (26)$$

Finally should be computed the turbulent frequency ω . For this purpose the reader should consult the equations on pages 84 and 85 of the ANSYS-CFX[®] manual (2006).

For more detailed information about the formulation of the above models should be consulted the ANSYS-CFX[®] manual (2006) and the literature cited herein. The formulation present in this manual is extensively used in the paper, considering that the CFX code was extensively used for all the reported numerical simulations. The books by Tennekes and Lumley (1972), Wilcox (1993); Versteeg and Malalasekera (1995) and Pope (2000) present the theory of turbulence modeling more deeply and can be consulted.

3. Setup of the numerical simulations

In this section are described all the computational conditions assumed in the numerical simulations. In Figures 1 and 2 are shown the two different computational domains used in simulations. The first one, (see Figure 1) it is composed by the inlet section (blue color), the two valve plates, the lateral walls and the outlet section (yellow color). The second domain (see Figure 2) it is composed by all these sections, including an opening section (green color), right after the plate diameter, D. In this case the outlet section is displayed after the opening section. The simulated geometry is composed from two valve plates with diameter D and a central orifice of the diffuser of diameter, d = 75 mm. The valve configuration is characterized by the diameters relation equals to D/d = 16. Each valve plate has a thickness of 25 mm. This is the height of the inlet region shown in Figures 1 and 2. The separation between the plates is equal to 10 mm. The computational geometry (Figures 1 and 2) were made rotating one lateral wall for 10°, making a three dimensional domain in the form of wedge. In Figures 1 and 2 are also shown six reed lines, denoting the position where were obtained the experimental profiles of the mean time local gas velocity along the plate radius and where will be compared the numerical results. Next are presented the other tested and assumed simulation conditions.

Figure 1

CFX®

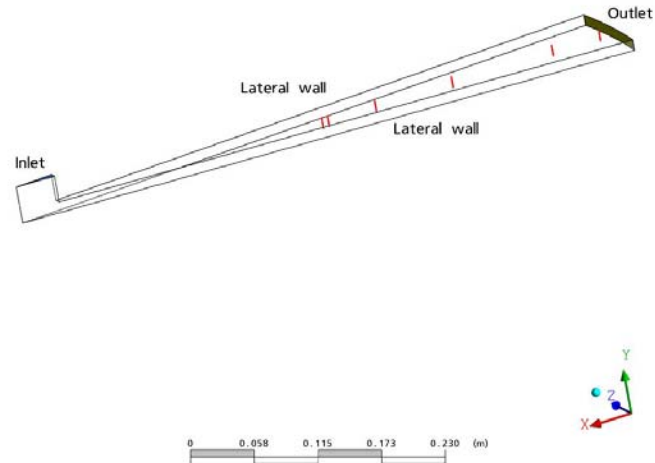


Figure 1. Computational domain considering the outlet section situated at the disc diameter.

Figure 2

CFX®

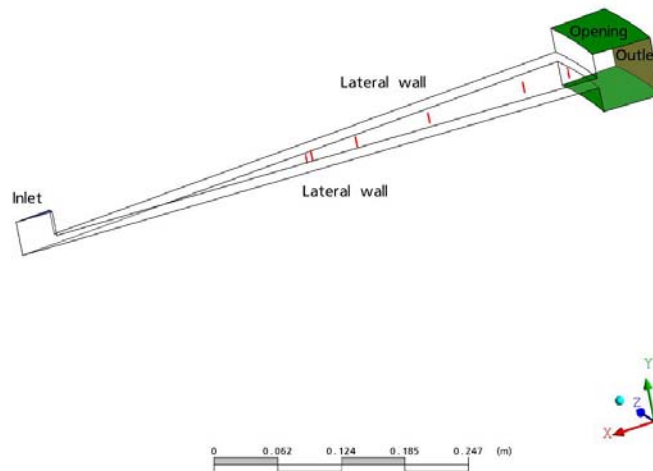


Figure 2. Computational domain considering an extension of the outlet section situated after the disc diameter.

Before the specification of the different boundary conditions assumed it should be specified which type of fluid was used for the simulations. In the case of the first geometry (Figure 1) the air was simulated as an incompressible fluid using the ANSYS-CFX® database (Air at 25°C fluid type from ANSYS-CFX® code). For the second geometry the air was considered as a compressible ideal fluid, but without any heat transfer with the walls and exits, assuming an air temperature equals to 298.15 K in the entire domain. In this case was computed the total energy equation considering the works terms due to the viscous dissipation. The interested reader should consult the ANSYS-CFX® manual (2006) to know what energy balance equation was used for this geometrical configuration.

With the exception of the above difference, regarding the kind of fluid used in the numerical simulations for each geometrical configuration, the other parameters were tested for both the geometrical configurations. Thus, besides the four different turbulence models, also where considered two different boundary conditions for the lateral walls of each

geometry, and three different inlet conditions depending on the inlet Reynolds number. The following boundary conditions (BC) were assumed:

- Inlet: It is specified the inlet velocity normal to the domain in the negative direction regarding the Y-axes (This velocity changes for each assumed inlet Reynolds number). It is assumed medium turbulence intensity, I , and, eddy viscosity ratio (see the ANSYS-CFX[®] manual). For the compressible fluid the inlet temperature is provided equal to 298.15 K.
- Outlet: It is assumed a subsonic flow with an average static pressure, over the entire outlet region, equal to 0.0 Pa. At the outlet the fluid can flow only out of the domain.
- Opening: It is assumed a relative pressure of 0.0 Pa and a static temperature equal to 298.15 K (This kind of BC is used only for the compressible fluid). At the openings the fluid can flow in and out of the computational domain. It is assumed medium turbulence intensity and eddy viscosity ratio.
- Lateral walls: For these walls are assumed two BC. One is a symmetry boundary condition, and the other is the free slip BC. At the symmetry BC the normal velocity at the wall is zero and the scalar variable gradients normal to the boundary are also zero. For the free slip walls, the velocity component parallel to the walls has a finite value, but the velocity normal to the wall, and the wall shear stress, are both set to zero. For the compressible fluid the walls are assumed as adiabatic.
- Other walls: In this case it is assumed the no slip BC, meaning that the fluid velocity at the wall has a zero value. For the compressible fluid the walls are assumed as adiabatic.

For all the turbulence models used in the work were assumed the ANSYS-CFX[®] software default turbulent wall functions. A detailed explanation about the formulation of these functions is presented in Volfang *et al.* (2002). The formulae are not presented here due to space limitations. The flow is simulated to obtain the steady state solution considering a maximum of 200 false time temporal iterations. These temporal iterations do not represent a truly transient flow behavior, and are used to achieve the steady state solution. In Table 1 is shown the main parameters assumed for the construction of computational meshes. The mesh used for the Fig. 1 geometry is much more refined than that used for Fig. 2 geometry. Nevertheless, even considering these two different meshes the Fig. 2 geometry leaded to better simulation results, indicating how the computational domain greatly influences the results and flow behavior. Due to the great number of performed simulations other computational meshes were not considered for the present work. The computations were run out in parallel using a cluster with eight processors.

Table 1. Computational mesh parameters.

| Geometry type | Total number of nodes | Total number of elements | Total number of faces |
|---------------|-----------------------|--------------------------|-----------------------|
| Figure 1 | 1,244,489 | 2,742,344 | 203,293 |
| Figure 2 | 343,008 | 956,403 | 66,946 |

4. Numerical results

In Figures 3 to 6 are shown the profiles of the mean time local gas velocity at different radial positions, considering the four turbulence models, the two different BC at the lateral walls and the two computational geometries considered in the paper (see Figures 1 and 2). In all figures are displayed the experimental data taken from Tabatabai and Pollard (1987) to be able to compare the numerical results. The displayed velocity profiles are disposed in the red lines shown in Figures 1 and 2. Now is performed a discussion considering the obtained results. It is very important to note that the results are shown partially, due to the quantity of parameters analyzed and the space limitation.

The first aspect that can be addressed is the performance of the turbulence models in relation to the experimental data. Considering all displayed results it is seen clearly that the $k-\epsilon$ and $RNG\ k-\epsilon$ models lead to simulation results, which are not in agreement with the experimental data and also with the physics of the flow. The more distorted results obtained with these two turbulence models are those shown in Figures 3 and 4, over all for the smaller and mean inlet Reynolds number values. For the high value Reynolds number (Figure 3c and 4c) the velocity profiles are more adequate, but very inaccurate at the discs walls, where the no slip BC it is not represented. This kind of behavior describes well that these two turbulence models are adequate for high Reynolds numbers in regions far away from the domain walls. In fact there are several modifications of the $k-\epsilon$ model for low Reynolds number flow simulation. Hrenya *et al.* (1995) presents a comparative study of ten different models of this type. However, even considering these low Reynolds number $k-\epsilon$ models, it is known that these models uses complex non-linear damping functions for the wall treatments, leading to very erroneous results. This conclusion can be extended even for high Reynolds number flows as can be see from Figures 3c and 4c, where these two models faults to catch the right behavior at the disc's walls. The same comments apply for the results displayed in Figures 5 and 6, obtained for other geometrical configuration and fluid model (compressible fluid). In this case, the velocity profiles are more coherent in relations to Figures 3 and 4 results, mainly at the centerline, but have a very poor behavior at the channel walls. In several works Churchill and coworkers (Churchill, 2000; and other related works) discussed and showed that the $k-\epsilon$ turbulence type of models have determined failures, because they use the concepts of eddy viscosity and mixing length to compute the turbulent viscosity. The failures are associated with the unbounded character of the eddy viscosity and mixing length at some locations of channels, and also with the assumption of negative values over some adjacent to the walls finite

regions, although the turbulent stresses remains well behaved. Considering all these comments and the presented results, it can be concluded that simulation results of the turbulent diffuser flow obtained with the $k-\epsilon$ and $RNG k-\epsilon$ should be treated with care, to avoid obtaining erroneous conclusions about the flow structures and main characteristics.

Now analyzing the results obtained for the SST and BSL models, can be said that both models allows obtaining numerical results physically coherent and generally very adequate in relation to the experimental data. However, some differences between these two turbulence models can be pointed out. In Figures 3 and 4 it is seen that there are shown results for the BSL model only for the smaller inlet Reynolds number ($Re_{in} = 19096$). In the case of the SST model, are displayed results only for Re_{in} equals to 19096 and 32804. The main reason for not to show the other results is that in these cases the code does not converge inside the number of temporal iterations fixed, equally to 200 iterations. These iterations are related to false time iterations to obtain a steady state solution. In the case of the BSL model, the time step was reduced to obtain a converged solution, considering the quantity of equations that should be solved for this model. When it is simulated the Figure 2 geometry and fluid model, the above two models converge, except the BSL model for $Re_{in} = 164441$. The same conditions where considered in this case.

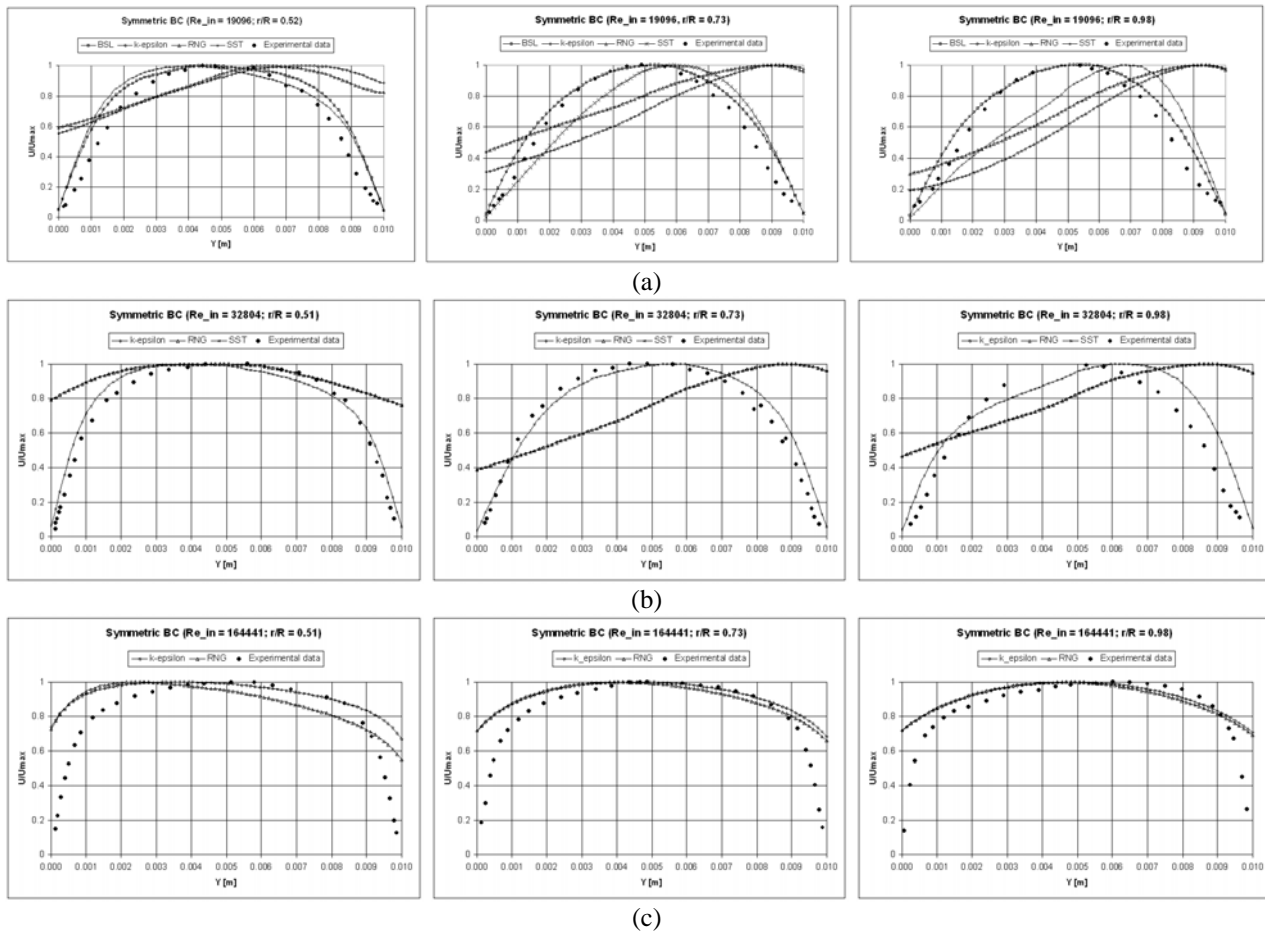


Figure 3. Mean velocity distribution across the discs gap at various radial locations, considering the geometry shown in Figure 1, the symmetric BC at the lateral walls and the four turbulence models. [(a) – $Re_{in} = 19096$; (b) – $Re_{in} = 32804$; (c) – $Re_{in} = 164441$].

Considering only the results displayed in Figures 3 and 4, it can be said that the BSL model leads to more correct results, at least for the low inlet Reynolds number ($Re_{in} = 19096$) for which both models can be compared. The more accentuated differences between the models, are observed at the radial coordinate $r/R = 0.98$, where the SST model presents a very not symmetric profile. This behavior is not correctly, because at this radial distance the flow dissipates the initial asymmetric due to the cross-stream momentum transfer as pointed out by Tabatabai and Pollard (1987). However, this does not means that the SST model leads to erroneous results for the other flow cases, as can be observed in Figures 3b and 4b. For this value of Re_{in} the SST model presents a more coherent behavior in relation to the experimental data, showing the asymmetry at $r/R = 0.98$ but, to a less extend.

For results showed in Figures 5 and 6, it is noted that both the models present a very similar behavior, showing small differences between each other and in comparison with the experimental data. For these simulations, the SST model converged for all the tested cases, contrary to the BSL model, which, does not converged for the high value of Re_{in} . Thus, even knowing that the BSL model is more universal, due to the use of transport equations for the Reynolds stress computations, the present results indicates that the SST model can be preferred for simulating different flow

conditions characteristics of a design phase of any engineering project. In fact, the *BSL* model is more time consuming than the *SST* model, leading in the case of Figures 5 and 6, to results that are very similar and of the same quality. In Table 2 are displayed values of the computational time for these two models for some of the performed simulations. As can be seen, the *SST* has a very small computational time regarding the *BSL* model. Considering this advantage of the *SST* model and the good results, which can be obtained with this model, it seems that this turbulence model is a good choice for numerically simulating the diffuser turbulent flow.

Table 2. Comparison of the running computational time for the *BSL* and *SST* models.

| Turbulence Model | $Re_{in} = 19096$ (Symm. BC) | $Re_{in} = 32804$ (Symm. BC) | $Re_{in} = 19096$ (Free BC) | $Re_{in} = 32804$ (Free BC) |
|------------------|------------------------------|------------------------------|-----------------------------|-----------------------------|
| <i>SST</i> | 42m58s | 47m4s | 43m41s | 46m45s |
| <i>BSL</i> | 1h2m59s | 1h4m6s | 1h3m5s | 1h3m51s |

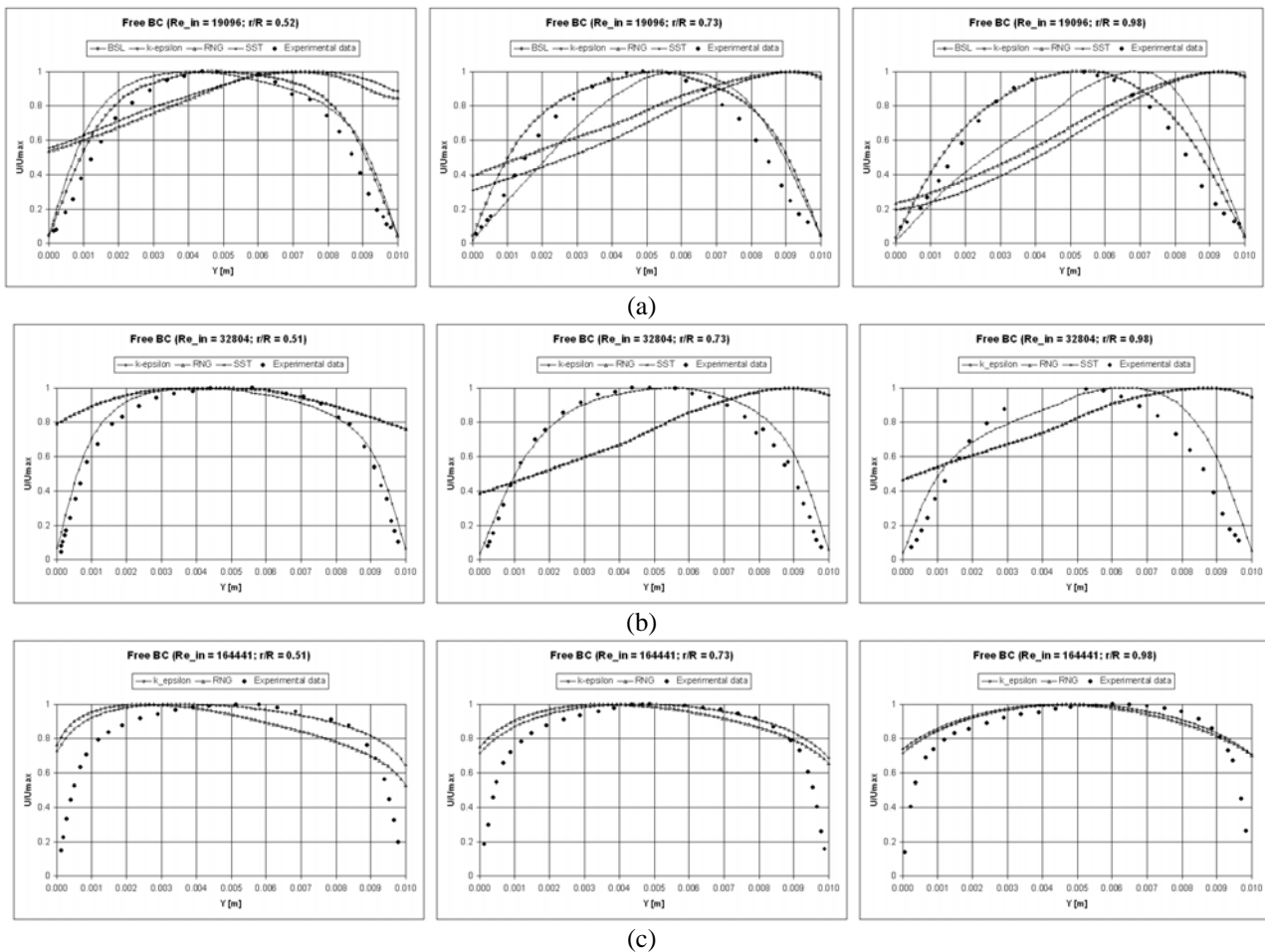


Figure (4). Mean velocity distribution across the discs gap at various radial locations, considering the geometry shown in Figure 1, the free slip BC at the lateral walls and the four turbulence models. [(a) – $Re_{in} = 19096$; (b) – $Re_{in} = 32804$; (c) – $Re_{in} = 164441$].

Focusing now on the influence of the type of BC applied for the lateral walls over the studied gas turbulent flow inside a diffuser, the results show that this influence is very small in all the analyzed cases. The only slightly differences are perceived for the results of $Re_{in} = 164441$ displayed in Figures 5c and 6c. As seen in these pictures, the *k-ε* and *RNG* *k-ε* models depend more on the type of this BC, than the *SST* model. Making a careful comparison it is seen that the symmetric type of BC is more adequate to the kind of flow simulated in comparison with the free slip type of BC. It should be commented that the use of these BCs is a necessary step in order to decrease the required computational time. The risk of this type of assumption is the lost of tri-dimensional flow effects or the formation of artificial flow structures. However, observing the obtained results, it is noted that in the kind of flow studied, these types of BC represent well the flow behavior.

A more pronounced influence over the diffuser turbulent flow is noted when is compared the kind of computational domain and fluid model used in the simulations. Comparing the results from Figures 3 and 4 with those represented in Figures 5 and 6, it is noted that the extended computational domain (see Figure 2) allows obtaining better computational results for all the tested turbulence models, including both the BC at the domain lateral walls. This points to the facts that the use of one or another computational domain is an important aspect to be taking into account when are

performed CFD numerical simulations. Many simulations in the literature, of problems similar to the present one, uses only the geometry shown in Figure 1, when the disc's radius is higher in relation to the diffuser orifice radius. Nevertheless, when turbulent flows are considered, as the present one, the type of computational geometry exerts a considerable influence over the simulation results. In the present case it is perceived that even if the flow have a symmetrical characteristics, properly of laminar flows near the domain exit, i.e., at largely values of the radial coordinate, the free stream turbulence can influence in a very high degree the numerical results. Note that the higher differences between the two types of computational domains are noted at the exits of the domains, namely at the $r/R = 0.98$ cross-section.

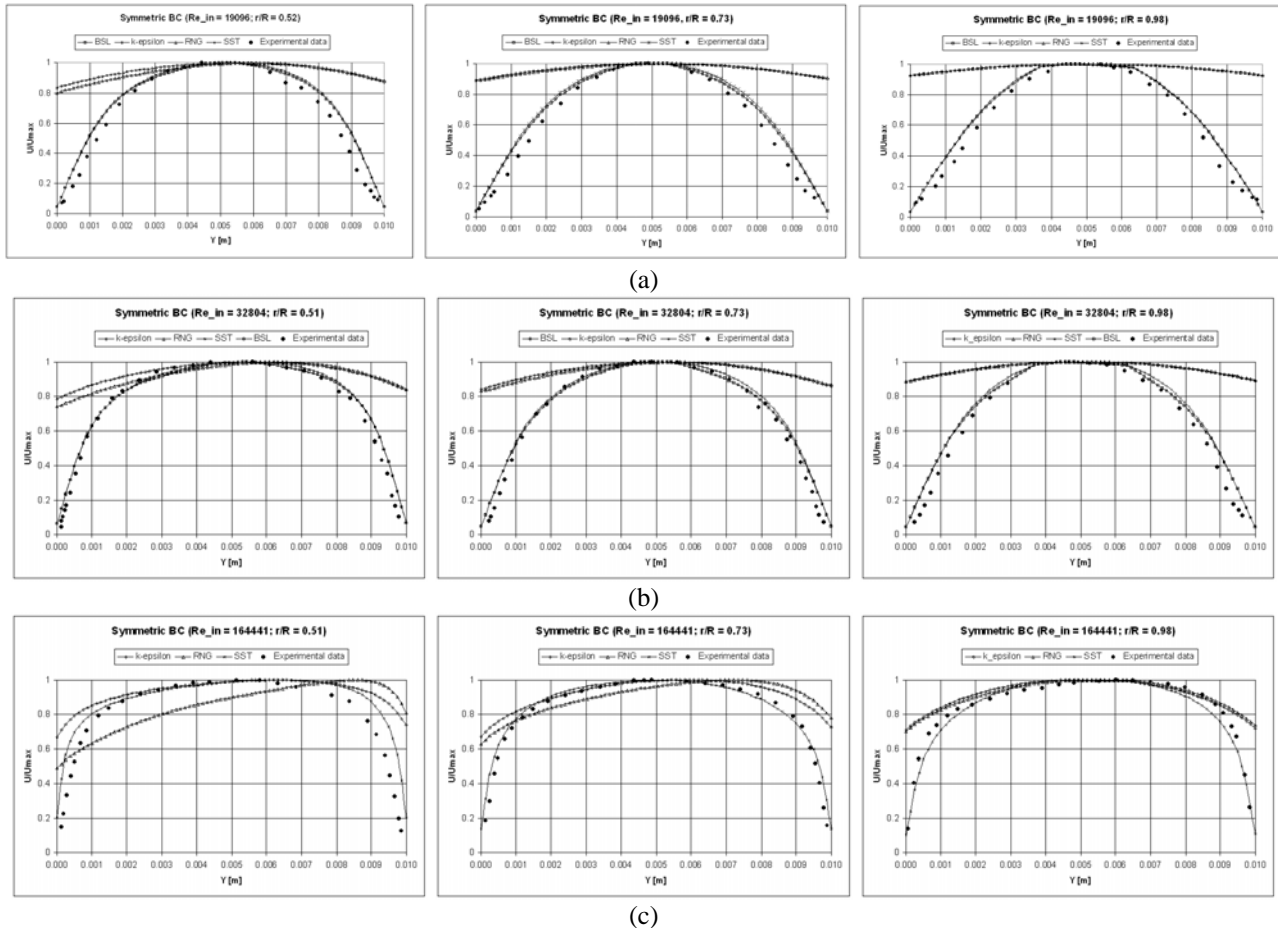


Figure 5. Mean velocity distribution across the discs gap at various radial locations, considering the geometry shown in Figure 2, the symmetric BC at the lateral walls and the four turbulence models. [(a) – $Re_{in} = 19096$; (b) – $Re_{in} = 32804$; (c) – $Re_{in} = 164441$].

Table 3. Values of the y^+ variable for the *RNG k-ε* and *SST* models and two Reynolds number values.

| Turbulence Model | $Re_{in} = 19096$ (Regions near inlet) | $Re_{in} = 19096$ (Regions near outlet) | $Re_{in} = 164441$ (Regions near inlet) | $Re_{in} = 164441$ (Regions near outlet) |
|------------------|--|---|---|--|
| <i>RNG k-ε</i> | $1.0 \leq y^+ \leq 3.8$ | $y^+ \leq 1.0$ | $7.7 \leq y^+ \leq 30.2$ | $y^+ \leq 7.7$ |
| <i>SST</i> | $1.5 \leq y^+ \leq 5.7$ | $y^+ \leq 1.5$ | $7.5 \leq y^+ \leq 30.3$ | $y^+ \leq 7.5$ |

For instance, should be noted, that besides the difference in the computational domain geometry in the present work are used two different fluid models. One is an incompressible and the other considers the compressibility effects on the flow turbulence. Thus, it cannot be associate all the reported results' differences only for the type of computational domain. Nevertheless, the simulations for the compressible fluid were performed assuming an adiabatic flow with the same inlet and outlet flow static temperatures. Considering that the flow velocities are not so high, it is seem, that the computational domain is the parameter, which is contributing more for the presented results' differences.

In Table 3 are presented some data regarding the value of y^+ at the walls for the *RNG k-ε* and *SST* models. There are not presented graphics due to paper space constraints. According to the ANSYS-CFX[®] manual it is recommended to have the following values of y^+ : $20 \leq y^+ \leq 100$ for wall functions (*RNG k-ε* model) and $y^+ \leq 2$ for low Reynolds numbers models (*SST* model). As can be seen from Table 3 the y^+ values should be improved for the *RNG k-ε* model. For the *SST* model the y^+ values are in better agreement with the recommendations, excepting for $Re_{in} = 164441$. In this case the mesh should be refined more in the regions near the diffuser inlet (extending up to the middle of the diffuser

radius). Table 3 results indicate that it is necessary to improve the computational mesh, mainly for the *RNG k-ε* and *k-ε* models to have better resolution of these models at the walls. Nevertheless these models lead to not physically coherent simulation results (see Figs. 3-6) even for $Re_{in} = 164441$ case, where y^+ values are inside the recommended interval. This fact validates the conclusions of the present work.

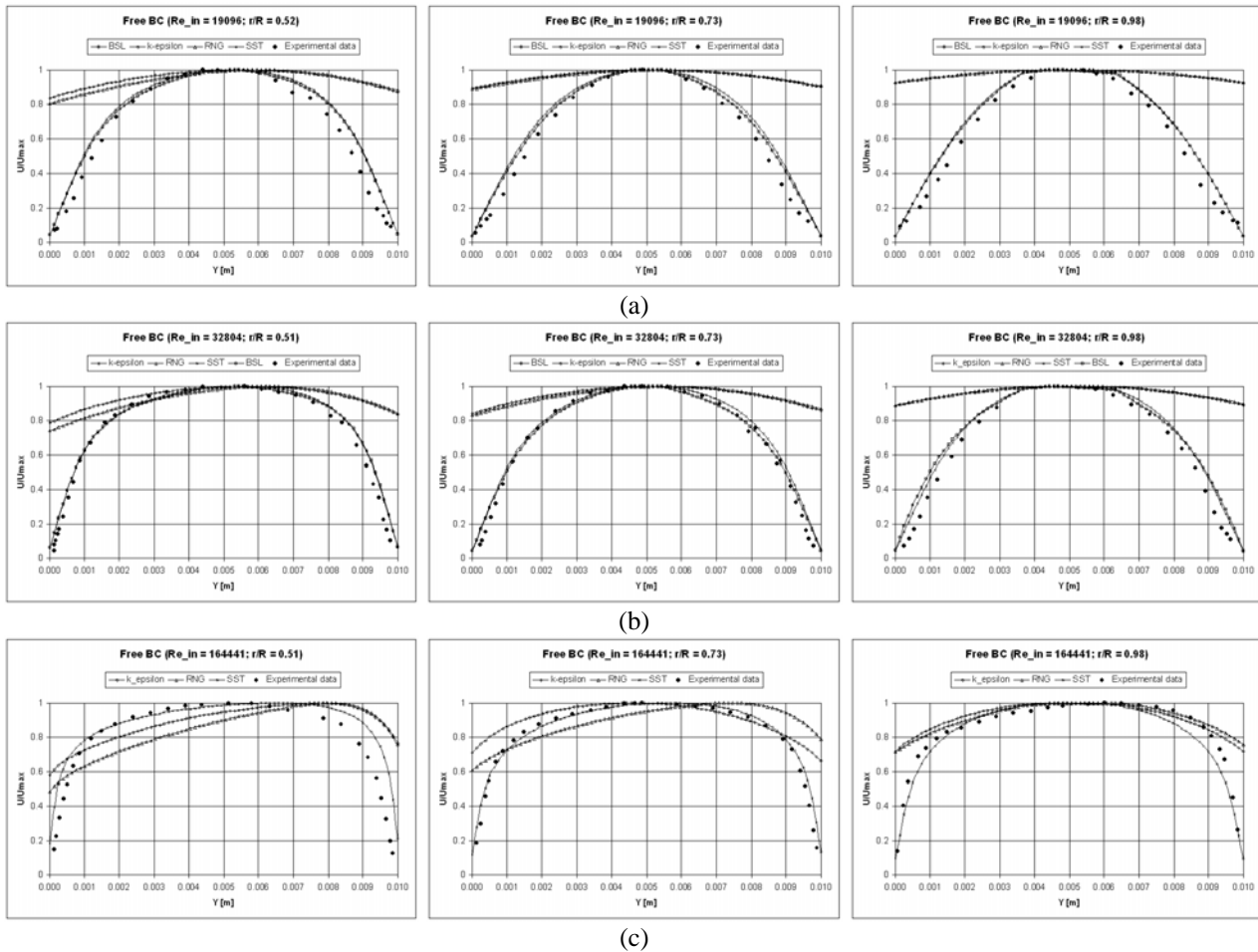


Figure 6. Mean velocity distribution across the discs gap at various radial locations, considering the geometry shown in Figure 2, the free slip BC at the lateral walls and the four turbulence models. [(a) – $Re_{in} = 19096$; (b) – $Re_{in} = 32804$; (c) – $Re_{in} = 164441$].

5. Conclusions

Taking into account the above discussion, it is seen that the use of one or another turbulence model, depend on a compromise between the quality of the results, the number of simulations needed and the geometrical and computational characteristics employed in the simulations. Using as a base the present simulation results can be affirmed that for the turbulent diffuser flow simulation the *SST* model is a good choice, considering the use of the *BSL* model for a comparative purpose for some simulation cases, when the converge is achieved. The use of the *k-ε* and *RNG k-ε* models is strongly not recommended, even is these models are more stable from the numerical point of view and consume less computational time. In any case, the obtained results with these two last models are not correct when compared with the experimental data and physically incorrect at the walls.

The obtained results confirm the poor influence exerted over the flow by the type of BC applied at the lateral walls. Nevertheless, it is recommended the use of the symmetric BC with base on the results showed for the *SST* model at $Re_{in} = 164441$ and Figure 2 geometry. Finally, it was found that the type of computational domain, can exert a significantly influence over the simulation results, even if the domains only differs in the exit zone configuration. It is very important to note, that for turbulent flows this region is characterized by complex flow structures and should be modeled with caution.

6. Acknowledgement

The authors fully acknowledge the support obtained from the Tecumseh do Brasil LTDA Company for the development of the present research work.

7. References

- ANSYS-CFX[®]-Solver Theory manual, Release 10.0, 1996.
- Churchill, S. W., 2000, "Progress in the Thermal Sciences: AIChE Institute Lecture", AIChE Journal, Vol.46, N^o9, 1704-1722.
- Cyklis, P., 1994, "CFD Simulation of the Flow Through Reciprocating Compressor Self-acting Valves", Proceedings of the International Compressor Engineering Conference, Purdue, pp. 427-432.
- Deschamps, C. J., Ferreira, R. T. S. and Prata, A. T., 1988, "Application of the k- ϵ Model to Turbulent Flow in Compressor Valves", Proceedings of the 2nd Brazilian Thermal Science Meeting, São Paulo, Brasil, pp. 259-262.
- Deschamps, C. J., Ferreira, R. T. S. and Prata, A. T., 1989, "Turbulent Flow Modeling in Presence of Stagnation Recirculation, Acceleration and Adverse Pressure Gradient", Proceedings of the X Brazilian Congress of Mechanical Engineering, Vol.1, pp. 57-60, (in Portuguese).
- Deschamps, C. J., Ferreira, R. T. S. and Prata, A. T., 1996, "Turbulent Flow Through Valves of Reciprocating Compressors", Proceedings of the International Compressor Engineering Conference, Purdue, pp. 377-382.
- Ervin, J. S., Suryanarayana, N. V. and Ng, H. C., 1989, "Radial, Turbulent Flow of a Fluid Between Two Coaxial Disks", ASME J. Fluids Engineering, Vol.111, pp. 378-383.
- Hayashi, S., Matsui, T. and Ito, T., 1975, "Study of Flow and Thrust in Nozzle-Flapper Valves", ASME J. of Fluid Engineering, Vol.97, pp. 39-50.
- Having, R. A., 2005, "Flow and Plate Motion in Compressor Valves", PhD. Thesis, University of Twente, Enschede, Netherlands, 156 p.
- Hrenya, C. M., Bolio, E. J., Chakrabarti, D and Sinclair, J. L., 1995, "Comparison of Low Reynolds Number $k-\epsilon$ Turbulence Models in Predicting Fully Developed Pipe Flow", Chemical Engineering Science, Vol.50, N^o12, pp. 1923-1941.
- Jackson, J. D. and Symmons, G. R., 1965, "An Investigation of Laminar Radial Flow Between Two Parallel Discs", Applied Scientific Research, Section A, Vol.15, pp. 59-75.
- Lauder, B. E. and Spalding, D. B., 1974, "The Numerical Computation of Turbulent Flows", Comput, Methods Appl. Mech. Eng., Vol.3, pp. 269-289.
- Lauder, B. E., Reece, G. J. and Rodi, W., 1975, "Progress in the Developments of a Reynolds-Stress Turbulence Closure", J. Fluid Mechanics, Vol.68, pp. 537-566.
- Livesey, J. L., 1960, "Inertia Effects in Viscous Flows", International J. Mechanical Science, Vol.1, pp. 84-88.
- Matos, F. F. S., Prata, A. T. and Deschamps, 1999, "Numerical Analysis of the Dynamic Behaviour of Plate Valves in Reciprocating Compressors", Proceedings ImechE Conference Transactions, C542/031, pp.453-462.
- Matos, F. F. S., Prata, A. T. and Deschamps, 2002, "Numerical Simulation of the Dynamics of Reed Type Valves", Proceedings of the International Compressor Engineering Conference, Purdue, C15-2.
- Menter, R. F., 1994, "Two-equation Eddy-viscosity Turbulence Models for Engineering Applications" AIAA Journal, Vol.32, N^o8, pp. 269-289.
- Moller, P. S., 1963, "Radial Flow Without Swirl Between Parallel Discs", The Aeronautical Quarterly, Vol.14, pp. 163-186.
- Ottitsch, F. and Scarpinato, P., 2000, "CFD a Viable Engineering Tool for Compressor Valve Design or Just a Toy?", Proceeding International Compressor Engineering Conference, Purdue, pp. 423-428.
- Perez-Segarra, C. D., Cadafalch, J., Rigola, J. and Oliva, A., 1999, "Numerical Study of Turbulent Fluid-flow Through Valves", Proceedings ImechE Conference Transaction, C542/021, pp. 399-408.
- Piechna, J. R. and Meier, G. E. A., 1986, "Numerical Investigation of Steady and Unsteady Flow in Valve Gap", International Compressor Engineering Conference, Purdue, pp. 1-14.
- Pope, S. B., 2000, "Turbulent Flows", Cambridge University Press, U.K., 771 p.
- Possamai, F. C., Ferreira, R. T. S. and Prata, A. T., 2001, "Pressure Distribution in Laminar Radial Flow Through Inclined Disks", International J. of Heat and Fluid Flow, Vol.22, pp. 440-449.
- Raal, J. D., 1978, "Radial Source Flow Between Parallel Discs", J. Fluid Mechanics, Vol.85, pp. 401-416.
- Savage, S. B., 1964, "Laminar Radial Flow Between Parallel Plates", ASME J. of Applied Mechanics, Vol.31, 594-596.
- Speziale, C. G., Sarkar, S. and Gatski, T.B., 1991, "Modelling the Pressure-Strain Correlation of Turbulence: an Invariant Dynamical Systems Approach", J. Fluid Mechanics, Vol.227, pp. 245-272.
- Tabatabai, M. and Pollard, A., 1987, "Turbulence in Radial Flow between Parallel Disks at Medium and Low Reynolds Numbers", J. Fluid Mechanics, Vol.185, pp. 483-502.
- Tennekes, H. and Lumley, J. L., 1972, "A First Course in Turbulence", MIT Press, Cambridge MA, p.
- Versteeg, H. K. and Malalasekera, W., 1995, "An Introduction to Computational Fluid Dynamics. The Finite Volume Method", Prentice Hall, U.K., 257 p.
- Volfang, V., Thomas, E. and Florian M., 2002, "Heat transfer predictions using advanced two-equation turbulence models." CFX Technical Memorandum-CFX-VAL10/0602.
- Wilcox, D. C., 1993, "Turbulence Modeling for CFD", DCW Industries, La Cañada, CA,
- Yakhot, V., Orszag, S. A., Thangam, S., Gatski, T. B. and Speziale, C. G., (1992), "Development of Turbulence Models for Shear Flows by a Double Expansion Technique", Physics of Fluids A, Vol.4, N^o7, pp. 1510-1520.